







Quantum error correction under numerically exact open-quantum-system dynamics

Aravind P. Babu ¹, Tuure Orell ¹, Vasilii Vadimov ², Wallace Teixeira ², Mikko Möttönen ^{2,3} and Matti Silveri ¹

¹Nano and Molecular Systems Research Unit, University of Oulu, P.O. Box 3000, FI-90014 Oulu, Finland

²QCD Labs, QTF Centre of Excellence, Department of Applied Physics, Aalto University, P.O. Box 13500, FI-00076 Aalto, Finland

³QTF Centre of Excellence, VTT Technical Research Centre of Finland Ltd., P.O. Box 1000, FI-02044 VTT, Finland



(Received 9 December 2022; accepted 25 October 2023; published 20 November 2023)

The known quantum error-correcting codes are typically built on approximative open-quantum-system models such as Born-Markov master equations. However, it is an open question how such codes perform in actual physical systems that, to some extent, necessarily exhibit phenomena beyond the limits of these models. To this end, we employ numerically exact open-quantum-system dynamics to analyze the performance of a five-qubit error-correction code where each qubit is coupled to its own bath. We first focus on the performance of a single error-correction cycle covering timescales and coupling strengths beyond those of Born-Markov models. We observe distinct power-law behavior of the error-corrected channel infidelity $\propto t^{2a}$: $a \lesssim 2$ in the ultrashort times $t < 3/\omega_c$ and $a \approx 1/2$ in the short-time range $3/\omega_c < t < 30/\omega_c$, where ω_c is the cutoff angular frequency of the bath. Furthermore, the observed scaling of the performance of error correction is found to be robust against various imperfections in physical qubit systems, such as perturbations in qubit-qubit coupling strengths and parametric disorder. For repeated error correction, we demonstrate the breaking of the five-qubit error-correction code and of the Born-Markov models if the repetition rate of the error-correction cycles exceeds $2\pi/\omega$ or the coupling strength $\kappa \gtrsim \omega/10$, where ω is the angular frequency of the qubit. Our results provide bounds of validity for the standard quantum error-correction codes and pave the way for applying numerically exact open-quantum-system methods for further studies of error correction beyond simple error models and for other strongly coupled many-body models.

DOI: [10.1103/PhysRevResearch.5.043161](https://doi.org/10.1103/PhysRevResearch.5.043161)

I. INTRODUCTION

One of the greatest milestones of quantum computing has been the experimental demonstration of quantum supremacy [1–3]. The practical use cases are yet to be demonstrated since it generally calls for higher qubit numbers and operational fidelity. Whereas physical qubits are constantly improving and it may be that they reach a level where currently known [4,5] or fully new algorithms yield practical quantum advantage, it is challenging to reach the required operational fidelity.

Quantum error correction [6–9] provides a theoretically established [10–14] but experimentally challenging [15–31] path to fault-tolerant and practically useful quantum computations. Notable approaches include the qubit-based repetition codes [7], surface codes [11,13,32], and color codes [12], as well as various bosonic codes [33,34]. Recently, experimental tests of the scaling of logical errors with increasing the code size have been reported [30] on the path to demonstrate major benefits of error correction.

Importantly, there remains a profound question to be answered along the path to practical error correction: Are the

relatively simple error models used in most theoretical studies of quantum error correction adequate? Namely, the usual local Born-Markov approach to open quantum systems [35] motivates an error model where Poisson-distributed bit and phase flips are applied on the individual physical qubits [36]. However, non-Markovian dynamics [37], global effects of the environment on the system [38,39], and system-environment correlations [40,41] are neglected in such approaches, which raises the concern of whether these phenomena can lead to small but significant errors in the logical qubits that need to operate at extremely high fidelity.

To this end, we analyze the performance of quantum error-correction codes beyond the simplified models of the open-quantum-system dynamics, and answer the question of what the validity limits are of quantum error correction subject to strong coupling and non-Markovian environments. We employ a numerically exact treatment for five physical qubits, each coupled to ohmic baths with the second-order Lorentz-Drude cutoff at angular frequency ω_c (Sec. II). Our setup is generic, allowing various possibilities for qubit-environment and qubit-qubit coupling beyond the approximate models.

By encoding quantum information into a five-qubit quantum error-correction code [14], we first assess the channel induced by the numerically exact model for a single error-correction cycle (Secs. III and IV). At ultrashort times $t < 3/\omega_c$ and short times $3/\omega_c < t < 30/\omega_c$, we observe apparent differences in the channel fidelity with respect to Born-Markov dynamics. We further validate our conclusions with

Published by the American Physical Society under the terms of the Creative Commons Attribution 4.0 International license. Further distribution of this work must maintain attribution to the author(s) and the published article's title, journal citation, and DOI.

an analytic model for the short-time dynamics. Finally, in Sec. V, we also apply repeated error correction and observe deviations from the infidelity given by Born-Markov results. However, when the repetition rate does not exceed $2\pi/\omega$ or the coupling strength $\kappa < 0.1\omega$, the experimentally relevant scenarios of Rabi-driven qubits, the Born-Markov approach, and hence the usually employed error model of bit and phase flips seem feasible to describe the quantum memory protected by the five-qubit code.

II. NUMERICALLY EXACT QUANTUM DYNAMICS FOR OPEN MANY-BODY SYSTEMS

We consider a system of five qubits, each coupled to its own decay channel modeled as a bath of bosonic modes. For generality, we also assume all-to-all hopping interaction between the qubits. The total system-bath Hamiltonian reads as $\hat{H} = \sum_{j=1}^5 (\hat{H}_j + \hat{H}_j^B)$ with the qubit parts

$$\hat{H}_j/\hbar = -\frac{\omega_j}{2}\hat{\sigma}_{zj} + J_j \sum_{i,j \neq i} (\hat{\sigma}_{+j}\hat{\sigma}_{-i} + \hat{\sigma}_{-j}\hat{\sigma}_{+i}), \quad (1)$$

where ω_j is the angular frequency of the qubit j , $\hat{\sigma}_{\alpha j}$ ($\alpha = x, y, z$) are the usual Pauli operators, and J_j determines the strength of the hopping interactions. The qubit-environment part is given by

$$\hat{H}_j^B/\hbar = \sum_k [\Omega_{kj}\hat{n}_{kj} + g_{kj}(\hat{b}_{kj} + \hat{b}_{kj}^\dagger)\hat{\sigma}_{xj}], \quad (2)$$

where Ω_{kj} is the angular frequency of the mode k of the j th bath, \hat{b}_{kj} and $\hat{n}_{kj} = \hat{b}_{kj}^\dagger\hat{b}_{kj}$ are its annihilation and number operator, respectively, and g_{kj} yields the coupling strength of the qubit j to the bath mode. The effect of each local bath can be completely described by its temperature T_j and the spectral density [42] of the form of $\mathcal{J}_j(\Omega) = \pi \sum_k g_{kj}^2 \delta(\Omega - \Omega_{kj})$, where $\delta(\Omega - \Omega_{kj})$ is the Dirac's delta function peaked at Ω_{kj} . We assume an ohmic-type distribution $\mathcal{J}_j(\Omega) = (\kappa_j/\omega_j)\Omega/(1 + \Omega^2/\omega_{cj}^2)^2$, where κ_j is the coupling strength of the qubit j to its bath and ω_{cj} is the bath cutoff frequency.

The cutoff frequency is introduced to make the model physically implementable. It is typically related to the fact that the nature of the environments may change at high frequencies. For example, in the case of superconducting qubits, the ohmic bath with a cutoff frequency can be an accurate model for a qubit coupled to its broadband drive line.

Typically, the Lindblad master equation method [35] is utilized to simulate the system-bath dynamics (see Appendix A). This approach is popular for its simplicity, but it is justified only for weak coupling between the qubits and their baths, short bath correlation time which restricts the bath temperature from below, and high-energy separation of the qubit states as compared to the resulting level broadening. For accurate simulations at strong coupling strengths or at short timescales, one needs to employ numerically exact methods [38,40,43,44]. Here, we use the stochastic Liouville equation with dissipation (SLED) which, for our multiqubit

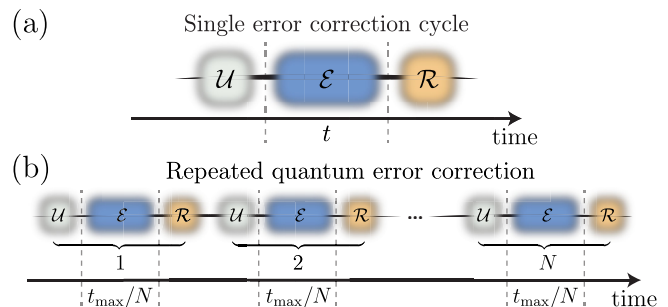


FIG. 1. Schematic of (a) the single-cycle and (b) the repeated error-correction processes. Here, \mathcal{U} is the encoding process, \mathcal{E} is the error process, and \mathcal{R} is the recovery process including the decoding operation also.

system (1), takes the form [40,43]

$$\frac{d\hat{\rho}}{dt} = \sum_{j=1}^5 \left\{ -\frac{i}{\hbar} [\hat{H}_j, \hat{\rho}] + i\kappa_j [\hat{\sigma}_{xj}, \{\hat{\sigma}_{yj}, \hat{\rho}\}] - \frac{\kappa_j}{\hbar\omega_j\beta_j} [\hat{\sigma}_{xj}, [\hat{\sigma}_{xj}, \hat{\rho}]] - i\xi_j(t) [\hat{\sigma}_{xj}, \hat{\rho}] \right\}, \quad (3)$$

where $\beta_j = 1/(k_B T_j)$, and the colored real-valued Gaussian noise $\xi_j(t)$ has the correlation function

$$\begin{aligned} \langle \xi_j(t)\xi_j(0) \rangle &= \frac{1}{\pi} \int_0^{+\infty} \mathcal{J}_j(\Omega) \left[\coth\left(\frac{\hbar\Omega\beta_j}{2}\right) - \frac{2}{\hbar\Omega\beta_j} \right] \cos(\Omega t) d\Omega. \end{aligned} \quad (4)$$

It is important that the full spectral density with the proper cut-off should be considered in Eq. (4), not just its low-frequency ohmic asymptotics. Owing to its stochastic nature and the need to average over many noise realizations, SLED is computationally quite an intensive method. By utilizing advanced techniques used in quantum many-body dynamics, such as Krylov subspaces and Magnus expansion, here, we go beyond the previous single- and two-qubit simulations [38], up to five qubits (see Appendix B for more details).

III. FIVE-QUBIT QUANTUM ERROR CORRECTION

To correct the errors caused by the local baths, we employ the five-qubit error-correction code introduced in Ref. [14]. We choose this code since it uses the minimum number of physical qubits to perfectly correct arbitrary single-qubit errors. The code operates with choosing a single main qubit such as $j = 3$ and adding four other qubits. A single error-correction cycle is characterized by an encoding process \mathcal{U} at the beginning of the time evolution, the error dynamics \mathcal{E} , followed by the recovery operation \mathcal{R} , as depicted in Fig. 1(a). Here, \mathcal{U} , \mathcal{E} , and \mathcal{R} are superoperators acting on the five-qubit system. The corresponding logical states and the Kraus map associated with \mathcal{R} are shown in Appendix C.

The recovery \mathcal{R} comprises the error detection through \mathcal{U}^{-1} and local measurements of the ancillae, their outcomes of which determine a unitary operation on the main qubit [14]. The recovery process uses no extra ancillae beyond the qubits

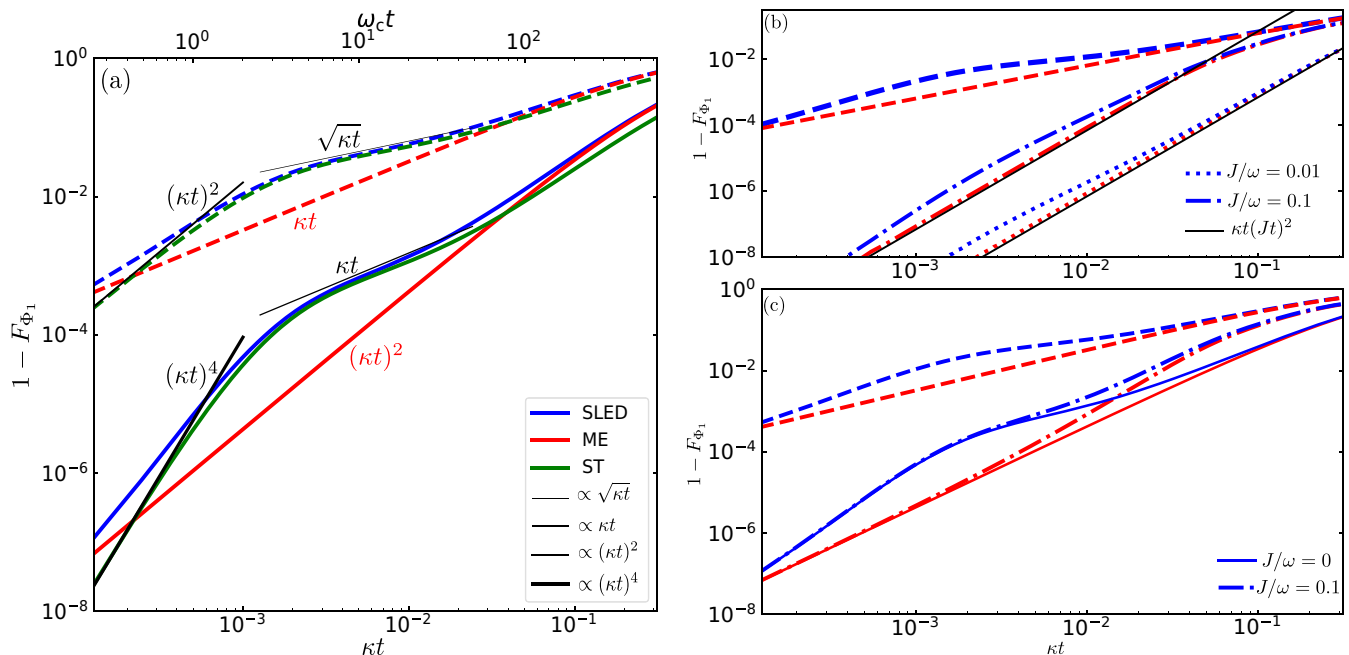


FIG. 2. Channel infidelity $1 - F_{\Phi_1}$ of the non-error-corrected channel (dashed lines) and the error-corrected channel (solid, dotted and dash-dotted lines) as a function of the time interval t from the encoding to the recovery, i.e., the duration of the error process, for the qubit-bath coupling strength $\kappa/\omega = 0.01$. Here we compare the results calculated by SLED (blue), the Lindblad master equation (ME, red), and the analytic short-time methods by Eq. (6) (ST, green). (a) All qubits are coupled to baths, $\kappa_j = \kappa$, without internal qubit-qubit coupling, $J_j/\omega = 0$. (b) Only a single qubit is coupled to a bath, $\kappa_3 = \kappa$, and all qubits are coupled to each other with internal qubit-qubit coupling parameters, $J_j = J$, where $J/\omega = 0.01$ (dotted lines) and 0.1 (dash-dotted lines). (c) All qubits are coupled to baths and the internal qubit-qubit coupling parameters are $J_j = J$ such that $J/\omega = 0$ (solid lines) and 0.1 (dash-dotted lines). Note that the non-error-corrected channel fidelity is independent of the value of J in (b) and (c). The qubits have identical frequencies, $\omega_j = \omega$. The baths are also identical with temperatures $\beta_j = 2$ and cutoff frequencies $\omega_{c_j}/\omega = 20$.

$j = 1, 2, 4$, and 5 . In realistic implementations, repeated cycles of error correction are usually required; see Fig. 1(b).

The five-qubit dynamics in the presence of repeated error correction can thus be ascribed to the quantum map $\Phi_N = (\mathcal{R}\mathcal{E}\mathcal{U})^N$, where N is the number of error correction cycles. Our focus here is to probe the deleterious effects on quantum error correction in the presence of an accurate description of open-quantum-system error dynamics \mathcal{E} promoting versatile decoherence, typically neglected in the simple error models, and not to model the actual physical qubit possibly affected by several additional error sources typically encountered in noisy intermediate-scale quantum devices such as gate, state preparation, and measurement errors [45]. Thus, we assume instantaneous and perfect encoding \mathcal{U} and recovery \mathcal{R} hereafter.

The performance of the five-qubit code is analyzed through the channel fidelity [46,47],

$$F_{\Phi_N} = \frac{1}{8} \sum_{j=0}^3 \text{Tr}[\hat{S}_j \Phi_N(\hat{S}_j)], \quad (5)$$

where the identity operator $\hat{S}_0 = |0_L\rangle\langle 0_L| + |1_L\rangle\langle 1_L|$, and the Pauli operators $\hat{S}_1 = |0_L\rangle\langle 1_L| + |1_L\rangle\langle 0_L|$, $\hat{S}_2 = -i|0_L\rangle\langle 1_L| + i|1_L\rangle\langle 0_L|$, and $\hat{S}_3 = |0_L\rangle\langle 0_L| - |1_L\rangle\langle 1_L|$ are defined in the logical qubit subspace $\{|0_L\rangle, |1_L\rangle\}$. The channel fidelity effectively quantifies the success of quantum information preservation under the action of the process Φ_N , so that successful error correction should produce values close to unity.

IV. SINGLE-CYCLE QUANTUM ERROR CORRECTION

We first analyze a single error-correction cycle and compute the channel fidelity with the SLED and the Lindblad models. We first assume that all the qubits and the corresponding baths are identical with no qubit-qubit couplings. Then, in Fig. 2(a), we show the infidelity $1 - F_{\Phi_1}$ of the quantum channel in Φ_1 without the recovery operation \mathcal{R} , i.e., the error channel infidelity (dotted lines) and the full channel that includes the recovery operation (solid lines) for $\kappa/\omega = 0.01$. The encoding and recovery process is assumed to be instantaneous, and time t is the waiting time between the encoding and recovery operation.

The error channel infidelity by the Lindblad model shows a linear dependence on κt as the single-qubit error probability per error-correction cycle is proportional to κt . The five-qubit error-correction protocol corrects all the first-order errors, i.e., a single Pauli operator action on a qubit, and leaves the higher-order errors uncorrected. Thus, the infidelity of the recovered channel essentially includes those uncorrected errors, and the recovered channel infidelity calculated with the Lindblad model is proportional to $(\kappa t)^2$.

The numerically exact open-quantum-system dynamics calculated with SLED considerably differs from the Lindblad predictions; see Fig. 2(a). In ultrashort times $\omega_c t \leq 3$, the error channel infidelity is proportional to $(\kappa t)^a$, where $a \leq 2$, whereas in short times, $3 < \omega_c t < 30$, the error channel infidelity is proportional to $(\kappa t)^b$, where $b \approx 1/2$. For the

long-time limit, $\omega_c t > 10$, the error channel infidelity shows a linear dependence on κt , same as the Lindblad results. Again the recovery process corrects the first-order errors and leaves the second-order errors uncorrected. Thus, recovery channel infidelity is proportional to: $(\kappa t)^{2a}$ at ultrashort times, $(\kappa t)^{2b}$ at short times, and $(\kappa t)^2$ at long times. In Appendix D, we provide estimates of infidelity for the strong coupling $\kappa/\omega = 0.1$. Interestingly, the exact open-quantum-system dynamics by SLED still demonstrates the observed power-law behavior for the ultrashort and short times for these parameters.

Deviation of the SLED results at short times is due to the universal decoherence, where the intrinsic dynamics of the system stays essentially frozen, and the high-frequency reservoir modes control the system dynamics [40,44,48]. We can obtain the resulting Liouvillian superoperator $\mathcal{L}^{\text{ST}}(\hat{\rho}) = d\hat{\rho}/dt$ of dynamics as

$$\mathcal{L}^{\text{ST}}(\hat{\rho}) = \sum_{j=1}^5 \frac{f'_j(t)\kappa_j}{\omega_j\pi} (\hat{\sigma}_{x_j}\hat{\rho}\hat{\sigma}_{x_j} - \hat{\rho}), \quad (6)$$

where $f'_j(t)$ is the time derivative of the integral average function,

$$f_j(t) = \frac{2\omega_j}{\kappa_j} \int_0^\infty d\Omega \frac{\mathcal{J}_j(\Omega)}{\Omega^2} \coth(\hbar\beta_j\Omega/2) \cos(\Omega t/2). \quad (7)$$

Here, we have extended the single-qubit short-time dynamics of Refs. [40,44]; see Appendix E for more details.

In ultrashort times, $t < 3/\omega_c$, $f(t) \approx -\omega_c^2 t^2/2$ and we can obtain the fidelity of the error channel as $F_{\Phi_1} = [1 + \exp(-\kappa\omega_c^2 t^2/\omega\pi)]^5/32$. Thus, infidelity $1 - F_{\Phi_1}$ is proportional to $(\kappa t)^2$ in ultrashort times. At later times, $t \leq 30/(\omega_c)$ infidelity shows roughly $\sqrt{\kappa t}$ behavior. The infidelity estimates with the analytic model are represented with green lines in Fig. 2(a). The SLED results closely follow the analytic dynamics, although there are some deviations in ultrashort times.

Next, we investigate the error-correction scheme in a more generic five-qubit setup by considering the case where the qubits are mutually interacting, that is, for $J \neq 0$ in Eq. (1). We begin with a simple model where only one qubit is coupled to the bath in the presence of all-to-all qubit coupling; see Fig. 2(b). Any error induced by the bath on a single qubit is fully correctable using the five-qubit error-correction code. However, due to the qubit-qubit interactions, an error event of losing an excitation may be accompanied by a phase flip explaining the observed $(Jt)^2\kappa t$ dependence in the recovered channel infidelity in the short-time regime; see Appendix F. At ultrashort times, the recovered channel infidelity is remarkably low, and hence contributions in this timescale can be neglected. Thus, the interaction between the qubits only changes the power-law behaviors at short and long timescales.

The channel infidelities for a fully generic case where all the qubits are coupled to their baths and $J \neq 0$ is shown in Fig. 2(c). The recovered channel infidelity starts deviating from the $J = 0$ results at short times, similar to previous results. However, these deviations are only significant for $J > \kappa$. In addition, we also examined the recovered channel infidelity for disorder in qubit frequencies, which also reproduces the same observed power-law behavior (see Appendix G).

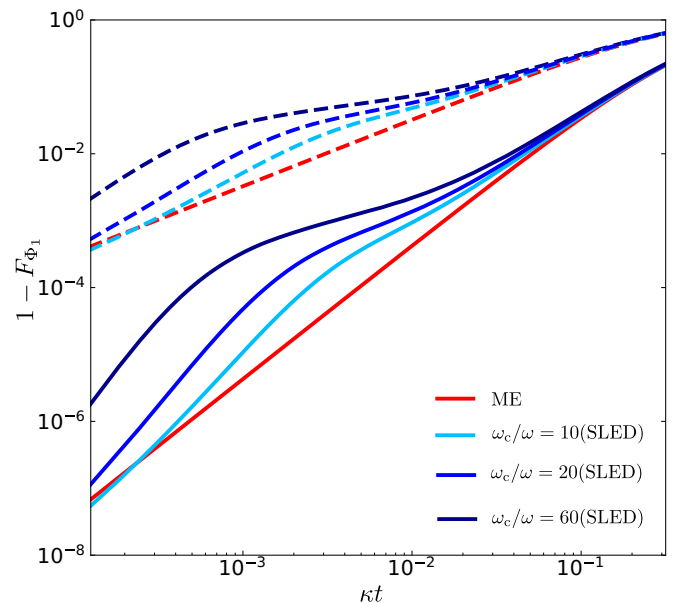


FIG. 3. Channel infidelity $1 - F_{\Phi_1}$ for the non-error-corrected channel (dashed lines) and the error-corrected channel (solid lines) as a function of the length of the time interval t from the encoding to the recovery for a Drude-type cutoff at the frequency $\omega_{c_j}/\omega = 10$ (cyan), 20 (blue), and 60 (dark blue). The Lindblad master equation results are independent of ω_c . The qubits and baths are assumed identical with $\omega_j = \omega$, $\kappa_j = \kappa = 0.01\omega$, $J/\omega = 0$, and $\beta_j = \beta = 2$.

To understand the dependence of the channel fidelity on the cutoff frequency, we compare the infidelities $1 - F_{\Phi_1}$ of the non-error-corrected and error-corrected channels for Drude-type cutoff at the frequencies $\omega_{c_j}/\omega = 10, 20$, and 60, shown in Fig. 3. Note that here we assume all the qubits and the corresponding baths are identical, with no qubit-qubit couplings. Results indicate that the general power-law behaviors do not vary with moderate change in the cutoff frequencies. An increase of ω_{c_j} shortens the ultrashort time part of the dynamics. However, the fidelity of the error channel decreases for short and ultrashort times owing to the enhancement of short-time decoherence.

V. REPEATED QUANTUM ERROR CORRECTION

Finally, we study what happens to the five-qubit quantum error correction at strong coupling κ , and find whether or not the strong environmental coupling is enough to demolish the benefits of active error correction. To this end, our focus is on the scheme of repeated quantum error correction, visualized in Fig. 1(b). We fix the total time interval $t_{\text{max}} = \kappa^{-1}$ and vary the number of error-correction cycles, N , within this interval. Here we assume identical qubits without qubit-qubit couplings. The expectation is that for a well-functioning error-correction process, an increase in the number of cycles, N , decreases the recovered channel infidelity for the final state at t_{max} .

Considering the Lindbladian description, the probability of the dominant uncorrected error per cycle is proportional to $(\kappa t)^2$, yielding that the channel infidelity at $\kappa t_{\text{max}} = 1$ scales as N^{-1} for $N \gg 1$ independent on the value of κ , as

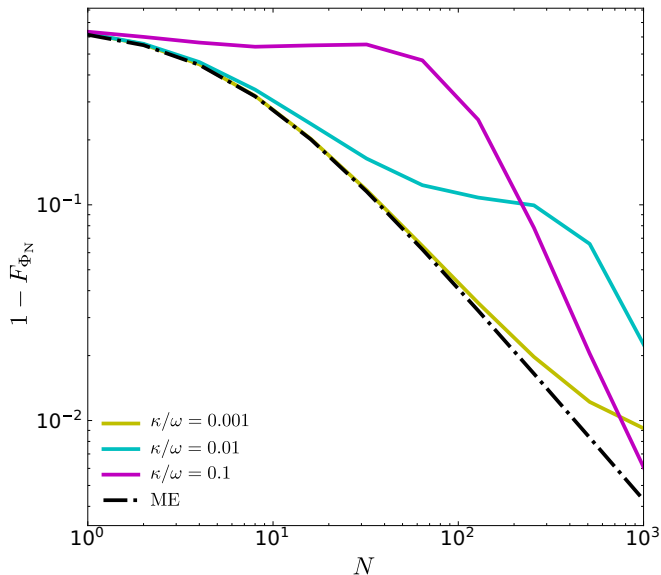


FIG. 4. Channel infidelity of the repeated error correction $1 - F_{\Phi_N}$ as a function of the number of the error correction cycles, N , within a fixed total time $t_{\max}\kappa = 1$ for different coupling strengths $\kappa/\omega = 0.001$ (yellow), 0.01 (blue), and 0.1 (magenta). The solid lines show the results computed by the SLED and the black dash-dotted line represents the κ -independent infidelity arising from the Lindblad master equation. We have $\omega_j = \omega$, $\kappa_j = \kappa$, $J_j = J = 0$, $\beta_j = \beta = 2$, and $\omega_{c_j} = \omega_c = 20\omega$.

shown in Fig. 4. To explore the effect of strong coupling, we compute in Fig. 4 the final infidelity of the repeated error-correction process using SLED at the limit of weak-, moderate-, and strong-coupling strengths, corresponding to $\kappa/\omega = 0.001$, 0.01 , and 0.1 . At the weak-coupling limit, the SLED infidelity shows only minor deviations from the scaling behavior predicted with the Lindblad model. Unsurprisingly, quantum error correction by the perfect five-qubit code functions adequately at weak qubit-environment coupling $\kappa/\omega \lesssim 0.001$. However, already at moderate values $\kappa/\omega = 0.01$, the infidelity starts to show plateauing as a function of N for $10 \lesssim N \lesssim 100$. The situation is even worse by strong coupling $\kappa/\omega = 0.1$, showing complete plateauing for $N \lesssim 100$. In both cases, the plateauing arises when the time interval between the recovery operations, $\delta t = t_{\max}/N$, is in the short-time domain where the error probability scales $(\kappa t)^{1/2}$. This result indicates that a simple distance-three error correction cannot overcome the fast occurrence of errors with probability $(\kappa t)^{1/2}$. When the repetition rate of error correction is very fast, corresponding to the ultrashort-time dynamics, we observe very favorable scaling of the infidelities as a function of N . However, the ultrashort dynamics corresponds to the case where the repetition rate of error correction is much faster than the qubit frequency, which contradicts the quantum speed limit. For example, for $\kappa/\omega = 0.1$, the favorable regime starts when $N > 10^2$, which yields $t < t_{\max}/N = \omega^{-1}/10$.

VI. CONCLUSIONS AND DISCUSSION

Typical quantum error-correction methods assume error models based on Born-Markov assumptions. We subjected

these assumptions to detailed scrutiny through numerically exact open-quantum-system error models, seeking the fundamental limits of the quantum error-correction processes in qubit-environment coupling strengths and applicable error-correction timescales.

We observed variations in the resulting quantum error-correction fidelity from the typical power-law behavior predicted by the Born-Markov model, specifically in the short-time domain $3 < \omega_c t < 30$ and ultrashort times where $\omega_c t < 3$, where ω_c is the cutoff frequency of the environment. These deviations arise from short-time universal decoherence induced by the bath modes. With a single recovery cycle of the five-qubit code, the first-order errors are corrected, rendering the second-order processes to subsequently dominate the remaining error channel. However, in the short times $3 < \omega_c t < 30$, the errors occur so frequently, scaling as $\sqrt{\kappa \delta t}$, that the recovery process of the distance $d = 3$ error-correction code is not suppressing them enough, best visualized in the repeated error-correction protocol. We believe that in this range, one would need at least $d = 5$ codes. Further inspection of higher distance codes under the exact open-quantum-system dynamics is left for future studies. Finally, through the repeated error-correction process, we demonstrate the breaking of the Born-Markov method and associated error-correction codes when the repetition rate exceeds $2\pi/\omega$ or the coupling strength $\kappa \gtrsim 0.1\omega$.

The consequences of the universal decoherence occur at such short timescales that they are beyond the current experimental state of the art and hence do not yield no-go results in practice for typical error-correction codes. In the future, it will be interesting to study the combined effect of gate errors and universal decoherence. To date, numerically exact open-quantum-system methods have been limited to few-qubit systems, but here we expanded them to genuine many-body systems. These techniques may find applications in simulations of ultra-strongly-coupled systems [49] or future development of novel quantum error-correction codes for other non-Markovian environments.

ACKNOWLEDGMENTS

We thank Jani Tuorila, Tapio Ala-Nissila, Jürgen Stockburger, and Joachim Ankerhold for useful discussions. We acknowledge funding by the Scientific Advisory Board for Defence (MATINE), Ministry of Defence of Finland, European Research Council under Consolidator Grant No. 681311 (QUESS) and Advanced Grant No. 101053801 (ConceptQ), and the Academy of Finland under Grants No. 316619 and No. 336810. The authors wish to acknowledge the CSC – IT Center for Science, Finland, for computational resources.

APPENDIX A: FIVE-QUBIT ERROR CORRECTION UNDER THE LINDBLAD DYNAMICS

The commonly used Born-Markov secular approximation reduces the joint unitary evolution of the extended system of qubits and their baths to the nonunitary evolution of the reduced density operator $\hat{\rho}$ of the five-qubit system governed

by the Lindblad master equation [35]

$$\frac{d\hat{\rho}}{dt} = \sum_{j=1}^5 \left\{ -\frac{i}{\hbar} [\hat{H}_j, \hat{\rho}] + \kappa_j [n_j(\omega_j) + 1] \mathcal{D}[\hat{\sigma}_{-j}] \hat{\rho} + \kappa_j n_j(\omega_j) \mathcal{D}[\hat{\sigma}_{+j}] \hat{\rho} \right\}, \quad (\text{A1})$$

where $\mathcal{D}[\hat{A}]\hat{\rho} = \hat{A}\hat{\rho}\hat{A}^\dagger - \hat{A}^\dagger\hat{A}\hat{\rho}/2 - \hat{\rho}\hat{A}^\dagger\hat{A}/2$, and $n_j(\Omega) = [1 - \exp(-\beta_j\hbar\Omega)]^{-1}$ is the average thermal occupation number of the j th bath with $\beta_j = 1/(k_B T_j)$. At low temperatures, $\hat{\sigma}_{j-}$ errors dominate over $\hat{\sigma}_{j+}$ errors, and we may neglect the contributions from $\hat{\sigma}_{j+}$. Consequently, the Lindblad master equation can be simply written as

$$\frac{d\hat{\rho}}{dt} = \sum_{j=1}^5 \left\{ -\frac{i}{\hbar} [\hat{H}_j, \hat{\rho}] + \kappa_j \mathcal{D}[\hat{\sigma}_{-j}] \hat{\rho} \right\}. \quad (\text{A2})$$

APPENDIX B: NUMERICAL TIME INTEGRATION FOR SLED

We use the stochastic Liouville equation with dissipation (SLED) to simulate numerically exact open-quantum-system dynamics, that is, error dynamics, which takes the form [40,43]

$$\frac{d\hat{\rho}}{dt} = \sum_{j=1}^5 \left\{ -\frac{i}{\hbar} [\hat{H}_j, \hat{\rho}] + i\kappa_j [\hat{\sigma}_{xj}, \{\hat{\sigma}_{yj}, \hat{\rho}\}] - \frac{\kappa_j}{\hbar\omega_j\beta_j} [\hat{\sigma}_{xj}, [\hat{\sigma}_{xj}, \hat{\rho}]] - i\xi_j(t) [\hat{\sigma}_{xj}, \hat{\rho}] \right\}, \quad (\text{B1})$$

where the colored real-valued Gaussian noise $\xi_j(t)$ has the correlation function

$$\langle \xi_j(t) \xi_j(0) \rangle = \frac{1}{\pi} \int_0^{+\infty} \mathcal{J}_j(\Omega) \cos(\Omega t) \times \left[\coth\left(\frac{\hbar\Omega\beta_j}{2}\right) - \frac{2}{\hbar\Omega\beta_j} \right] d\Omega. \quad (\text{B2})$$

The problem can be cast into the form

$$\frac{d}{dt} \mathbf{v}(t) = \mathbf{M}(t) \mathbf{v}(t), \quad (\text{B3})$$

where $\mathbf{v}(t)$ is the unknown vector, and $\mathbf{M}(t)$ is the matrix determining the problem. In our case, $\mathbf{v}(t)$ is the vectorized form of the density operator and $\mathbf{M}(t)$ is the matrix form of the superoperator defining the SLED. If one knows the vector $\mathbf{v}(t)$ at time t , the solution after a short time step δt can be obtained with the Magnus expansion,

$$\mathbf{v}(t + \delta t) = e^{\mathbf{A}(t+\delta t)} \mathbf{v}(t), \quad (\text{B4})$$

where the matrix $\mathbf{A}(t + \delta t)$ can be written in terms of univariate integrals [50],

$$\mathbf{A}(t + \delta t) = \delta t \mathbf{B}_0(t) + (\delta t)^2 [\mathbf{B}_0(t), \mathbf{B}_1(t)] + \mathcal{O}[(\delta t)^5], \quad (\text{B5})$$

with help of the matrices $\mathbf{B}_j(t)$,

$$\mathbf{B}_j(t) = \frac{1}{(\delta t)^{j+1}} \int_{-\delta t/2}^{\delta t/2} d\tau \tau^j \mathbf{M}\left(t + \frac{\delta t}{2} + \tau\right). \quad (\text{B6})$$

It turns out that it is sufficient to terminate the series after the first term and write the solution as

$$\mathbf{v}(t + \delta t) = e^{\delta t \mathbf{B}_0(t)} \mathbf{v}(t). \quad (\text{B7})$$

Now, for the SLED, one requires a small time step and the bottleneck of the above method is the calculation of the matrix exponential. For large and sparse systems, it can be efficiently implemented with the Krylov subspace method. For a small time step δt , the matrix $\mathbf{B}_0(t)$ and the vector $\mathbf{v}(t)$ can be accurately expressed in the m -dimensional Krylov subspace, with $m \ll \dim \mathbf{B}_0$. This subspace is spanned by the vectors

$$\{\mathbf{v}(t), \mathbf{B}_0(t)\mathbf{v}(t), \mathbf{B}_0^2(t)\mathbf{v}(t), \dots, \mathbf{B}_0^{m-1}(t)\mathbf{v}(t)\}.$$

Orthonormalizing this subspace results in a unitary matrix,

$$\mathbf{K}_m = (\mathbf{u}_1 \quad \mathbf{u}_2 \quad \mathbf{u}_3 \quad \dots \quad \mathbf{u}_m), \quad (\text{B8})$$

with which one can express the original matrix $\mathbf{B}_0(t)$ as a $m \times m$ dimensional matrix,

$$\mathbf{B} = \mathbf{K}_m^\dagger \mathbf{B}_0 \mathbf{K}_m, \quad (\text{B9})$$

with which one can approximately express the time evolution as

$$\mathbf{v}(t + \delta t) \approx \mathbf{K}_m e^{\delta t \mathbf{B}} \mathbf{K}_m^\dagger \mathbf{v}(t), \quad (\text{B10})$$

so that now we only need to calculate the matrix exponential of a small $m \times m$ matrix, instead of the full one. The orthogonalization of the subspace for a non-Hermitian matrix can be performed with the Arnoldi iteration, where one first constructs an $(m+1) \times m$ upper Hessenberg matrix $\tilde{\mathbf{B}}$ and $d \times (m+1)$ -dimensional matrix \mathbf{K}_{m+1} , where d is the dimension of the original matrix \mathbf{B}_0 . This can be done with the Gram-Schmidt orthogonalization,

$$m_{j+1,j} \mathbf{u}_{j+1} = \mathbf{B}_0 \mathbf{u}_j - \sum_{i=1}^j m_{i,j} \mathbf{u}_i, \quad m_{ij} = (\mathbf{B}_0 \mathbf{u}_i)^\dagger \mathbf{u}_j, \quad (\text{B11})$$

where $m_{i,j}$ are the elements of the matrix $\tilde{\mathbf{B}}$. The desired matrices can then be obtained by discarding the last row of $\tilde{\mathbf{B}}$ and the last column of \mathbf{K}_{m+1} .

APPENDIX C: DETAILS OF ENCODING AND RECOVERY PROTOCOL FOR THE FIVE-QUBIT CODE

In the five-qubit code [14], the encoding \mathcal{U} uses a sequence of nonlocal gates to encode the state of the main qubit into the logical subspace $\{|0_L\rangle, |1_L\rangle\}$, where

$$\begin{aligned} |0_L\rangle &= (-|00000\rangle + |00110\rangle + |01001\rangle + |01111\rangle \\ &\quad - |10011\rangle + |10101\rangle + |11010\rangle + |11100\rangle) / \sqrt{8}, \\ |1_L\rangle &= (-|11111\rangle + |11001\rangle + |10110\rangle + |10000\rangle \\ &\quad + |01100\rangle - |01010\rangle - |00101\rangle - |00011\rangle) / \sqrt{8}. \end{aligned} \quad (\text{C1})$$

A single recovery stage considered in the simulations of the main text can be written as the following Kraus map:

$$\mathcal{R}(\hat{\rho}) = \sum_{k=0}^{15} \hat{R}_k \hat{U}^\dagger \hat{\rho} \hat{U} \hat{R}_k^\dagger, \quad (\text{C2})$$

where \hat{U} is the unitary operator associated to the encoding process \mathcal{U} yielding the codewords $|0_L\rangle$ and $|1_L\rangle$; see Ref. [14]. In Eq. (C2), the operators $\{\hat{R}_k\}$ account for projective measurements of the auxiliary qubits $j = 1, 2, 4,$ and 5 in the computational basis, whose outcomes drive a unitary operation to correct the state of the main qubit, $j = 3$. To carry on the next recovery cycles, the auxiliary qubits are then reset to the state $|0000\rangle_{1245}$. Therefore, the operators $\{\hat{R}_k\}$ can be explicitly written as

$$\begin{aligned}
 \hat{R}_0 &= |00\rangle_{12}\langle 00| \otimes \hat{I}_3 \otimes |00\rangle_{45}\langle 00|, \\
 \hat{R}_1 &= |00\rangle_{12}\langle 00| \otimes \hat{\sigma}_{z3} \otimes |00\rangle_{45}\langle 01|, \\
 \hat{R}_2 &= |00\rangle_{12}\langle 00| \otimes \hat{I}_3 \otimes |00\rangle_{45}\langle 10|, \\
 \hat{R}_3 &= |00\rangle_{12}\langle 00| \otimes \hat{I}_3 \otimes |00\rangle_{45}\langle 11|, \\
 \hat{R}_4 &= |00\rangle_{12}\langle 01| \otimes \hat{I}_3 \otimes |00\rangle_{45}\langle 00|, \\
 \hat{R}_5 &= |00\rangle_{12}\langle 01| \otimes \hat{\sigma}_{z3} \otimes |00\rangle_{45}\langle 01|, \\
 \hat{R}_6 &= |00\rangle_{12}\langle 01| \otimes \hat{\sigma}_{x3} \otimes |00\rangle_{45}\langle 10|, \\
 \hat{R}_7 &= |00\rangle_{12}\langle 01| \otimes \hat{\sigma}_{x3} \otimes |00\rangle_{45}\langle 11|, \\
 \hat{R}_8 &= |00\rangle_{12}\langle 10| \otimes \hat{I}_3 \otimes |00\rangle_{45}\langle 00|, \\
 \hat{R}_9 &= |00\rangle_{12}\langle 10| \otimes \hat{\sigma}_{x3} \otimes |00\rangle_{45}\langle 01|, \\
 \hat{R}_{10} &= |00\rangle_{12}\langle 10| \otimes \hat{\sigma}_{z3} \otimes |00\rangle_{45}\langle 10|, \\
 \hat{R}_{11} &= |00\rangle_{12}\langle 10| \otimes \hat{\sigma}_{x3} \otimes |00\rangle_{45}\langle 11|, \\
 \hat{R}_{12} &= |00\rangle_{12}\langle 11| \otimes \hat{\sigma}_{z3} \otimes |00\rangle_{45}\langle 00|, \\
 \hat{R}_{13} &= |00\rangle_{12}\langle 11| \otimes \hat{\sigma}_{x3}\hat{\sigma}_{z3} \otimes |00\rangle_{45}\langle 01|, \\
 \hat{R}_{14} &= |00\rangle_{12}\langle 11| \otimes \hat{\sigma}_{x3} \otimes |00\rangle_{45}\langle 10|, \\
 \hat{R}_{15} &= |00\rangle_{12}\langle 11| \otimes \hat{\sigma}_{z3} \otimes |00\rangle_{45}\langle 11|, \tag{C3}
 \end{aligned}$$

where \hat{I}_3 is the identity operator and $\hat{\sigma}_{\alpha 3}$ ($\alpha = x, y, z$) are the Pauli matrices for qubit 3.

APPENDIX D: CHANNEL FIDELITY FOR A FIVE-QUBIT SETUP WITH STRONG SYSTEM-ENVIRONMENT COUPLING

Here, we present the infidelity estimates for relatively strong coupling, i.e., $\kappa/\omega = 0.1$. The qubits and baths are assumed identical with $\omega_j = \omega, \kappa_j = \kappa$, and $\beta_j = \beta = 2$. Figure 5 shows the infidelity estimates calculated with SLED (blue), the Lindblad master equation (ME, red), and the analytic short-time methods (ST, green). Similar to the previous case, SLED exhibits deviations for ultrashort and short times. However, the channel infidelity arising from this short-time dynamics at $t \approx 1/\omega_c$ appears to be 100 times greater than that of the case in Fig. 2(a) with $\kappa/\omega = 0.01$.

APPENDIX E: ANALYTIC MODEL FOR THE SHORT-TIME ERROR DYNAMICS

The short-time decoherence in the case of a single qubit interacting with a bosonic bath has already been demonstrated in Refs. [40,44]. Let us first analyze a single qubit in the five-qubit setting and extend it to the whole system later.

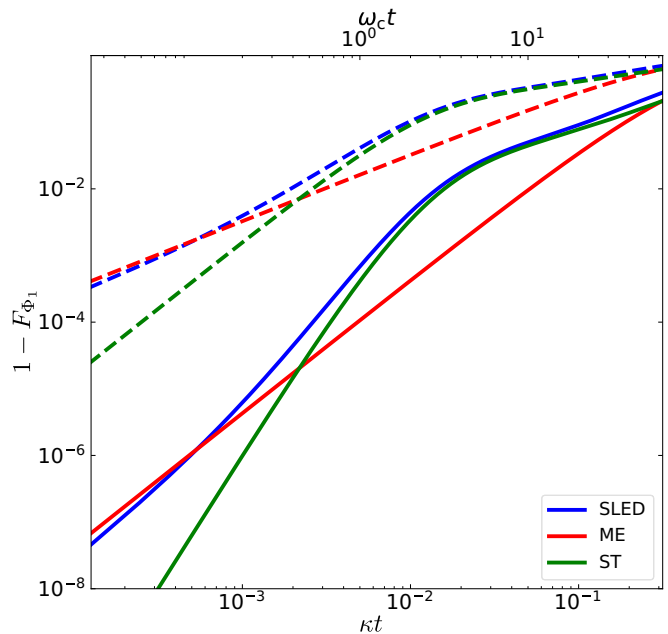


FIG. 5. Channel infidelity $1 - F_{\Phi_1}$ for the non-error-corrected channel (dashed lines) and the error-corrected channel (solid lines) as a function of the length of the time interval t from the encoding to the recovery. Here we compare the results calculated by SLED (blue), the Lindblad master equation (ME, red), and the analytic short-time methods (ST, green). The qubits and baths are assumed identical with $\omega_j = \omega, \kappa_j = \kappa = 0.1\omega, J/\omega = 0$, and $\beta_j = \beta = 2$.

In the early-time limit, the system dynamics remains frozen and high-frequency environmental modes control the dynamics. Thus, we completely ignore the system Hamiltonian and obtain the elements of the reduced density matrix in the eigenbasis of the operator $\hat{\sigma}_{xj}$ as [40,44]

$$\begin{aligned}
 \langle n|\hat{\rho}^j(t)|m\rangle &= \langle n|\hat{\rho}_S(0)|m\rangle \exp\left\{\frac{\kappa_j}{2\pi\omega_j}[i(n^2 - m^2)\phi_j(t) \right. \\
 &\quad \left. - (n - m)^2 f_j(t)\right\}, \tag{E1}
 \end{aligned}$$

where $f_j(t)$ and $\phi_j(t)$ are integral average functions and which take the form of

$$\begin{aligned}
 f_j(t) &= \frac{\omega_j}{\kappa_j} \int_0^\infty d\Omega \frac{\mathcal{J}_j(\Omega)}{\Omega^2} \coth\left(\frac{\hbar\beta_j\Omega}{2}\right) [1 - \cos(\Omega t)], \\
 \phi_j(t) &= \frac{\omega_j}{\kappa_j} \int_0^\infty d\Omega \frac{\mathcal{J}_j(\Omega)}{\Omega^2} [\Omega t - \sin(\Omega t)]. \tag{E2}
 \end{aligned}$$

Using the eigenstate expansion of $\hat{\sigma}_{xj} = \sum_n n|n\rangle\langle n|$, we can write the early-time evolution operator $\mathcal{L}^{\text{ST}}(\hat{\rho}^j)$ as

$$\begin{aligned}
 \mathcal{L}^{\text{ST}}(\hat{\rho}^j) &= \frac{i\phi'(t)\kappa}{2\pi\omega_j} [(\hat{\sigma}_{xj})^2, \hat{\rho}] \\
 &\quad + \frac{f'_j(t)\kappa_j}{2\pi\omega_j} [2\hat{\sigma}_{xj}\hat{\rho}^j\hat{\sigma}_{xj} - (\hat{\sigma}_{xj})^2\hat{\rho}^j - \hat{\rho}^j(\hat{\sigma}_{xj})^2], \tag{E3}
 \end{aligned}$$

where $\mathcal{L}^{\text{ST}}(\hat{\rho}^j) = d\hat{\rho}^j/dt$. We can then write the time evolution operator for the whole system as

$$\mathcal{L}^{\text{ST}}(\hat{\rho}) = \sum_{j=1}^5 \frac{f'_j(t)\kappa_j}{\pi\omega_j} (\hat{\sigma}_{xj}\hat{\rho}\hat{\sigma}_{xj} - \hat{\rho}). \quad (\text{E4})$$

APPENDIX F: GENERATION OF UNCORRECTABLE ERRORS VIA QUBIT-QUBIT INTERACTIONS

Using the Lindblad master equation (A2), we can write the approximated, time-evolved density operator in terms of Kraus operator representation as

$$\hat{\rho}(t) \approx \sum_{l=0,1} \hat{\rho}_l(t) = \sum_{l=0,1} \sum_{j=0}^5 \hat{E}_{lj} \hat{U}_H \hat{\rho}(0) \hat{U}_H^\dagger \hat{E}_{lj}^\dagger, \quad (\text{F1})$$

where $\hat{E}_{l=0,1}$ are the Kraus operators corresponding to zero or one error and \hat{U}_H is the unitary operator arising from the system Hamiltonian. We first consider the $\hat{\sigma}_-$ errors due to Kraus operator $\hat{E}_{1j} = \sqrt{\kappa t} \hat{\sigma}_j$ under the weak-coupling approximation.

Let us analyze the error process for a state $|\psi(0)\rangle = a_0|0_L\rangle + a_1|1_L\rangle$. Initially, the system evolves with a unitary operator $\hat{U}_H(t)$, and at time $t = \delta t$, single $\hat{\sigma}_-$ error occurs on qubit k with probability $\kappa\delta t$. We assume that the error is instantaneous and the system continues its unitary evolution immediately after the error event. Thus, taking into account just the error process, the initial state evolves to

$$|\psi(t)\rangle = \hat{U}_H(t - \delta t) \sqrt{\kappa\delta t} \hat{\sigma}_k \hat{U}_H(\delta t) |\psi(0)\rangle, \quad (\text{F2})$$

and, after phase recovery,

$$\begin{aligned} |\psi(t)\rangle &= \hat{U}_H(-t) \hat{U}_H(t - \delta t) \sqrt{\kappa\delta t} \hat{\sigma}_k \hat{U}_H(\delta t) |\psi(0)\rangle \\ &= \sqrt{\kappa t} \hat{U}_H(-\delta t) \hat{\sigma}_k \hat{U}_H(\delta t) |\psi(0)\rangle \\ &= \sqrt{\kappa\delta t} e^{i\hat{H}\delta t/\hbar} \hat{\sigma}_k e^{-i\hat{H}\delta t/\hbar} |\psi(0)\rangle. \end{aligned} \quad (\text{F3})$$

Note that $|\psi(t)\rangle$ in Eq. (F2) does not include the final state with no error event occurring. However, this part of the final state is irrelevant to the fidelity estimates. The exponential part can be expanded using the Baker-Campbell-Hausdorff formula,

$$\begin{aligned} &e^{i\hat{H}\delta t/\hbar} \hat{\sigma}_k e^{-i\hat{H}\delta t/\hbar} \\ &= \hat{\sigma}_k + \frac{i\delta t}{\hbar} [\hat{H}, \hat{\sigma}_k] - \frac{(\delta t)^2}{\hbar^2} [\hat{H}, [\hat{H}, \hat{\sigma}_k]] + \dots \\ &= \hat{\sigma}_k + i\delta t \omega_k \hat{\sigma}_k + iJ_k \delta t \sum_i \hat{\sigma}_{zk} \hat{\sigma}_{-i} + \mathcal{O}(\delta t)^2 \\ &= e^{i\omega_k \delta t} \left(\hat{\sigma}_k + iJ_k \delta t \sum_i \hat{\sigma}_{zk} \hat{\sigma}_{-i} \right) + \mathcal{O}(\delta t)^2, \end{aligned} \quad (\text{F4})$$

and the state after the phase recovery is, up to the second order in δt ,

$$|\psi(t)\rangle \approx \sqrt{\kappa\delta t} e^{i\omega_k \delta t} [\hat{\sigma}_k + iJ_k \delta t \sum_i \hat{\sigma}_{zk} \hat{\sigma}_{-i}] |\psi(0)\rangle. \quad (\text{F5})$$

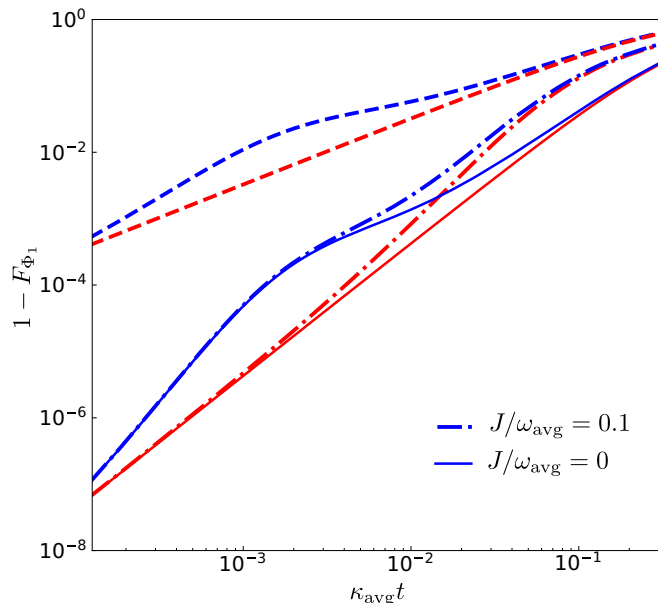


FIG. 6. Channel infidelity $1 - F_{\Phi_1}$ for the non-error-corrected channel (dashed lines) and the error-corrected channel (solid lines) as a function of the length of the time interval t from the encoding to the recovery. We compare the results calculated by SLED (blue) and the Lindblad master equation (ME, red). The qubits and baths are assumed to be nonidentical with an average qubit angular frequency $\omega_{\text{avg}} = \omega$ and 20% disorder, an average $\kappa_{\text{avg}} = \kappa = 0.01\omega$ and 20% disorder, and $\beta_j = \beta = 2$.

The approximate Kraus operator for the channel $\tilde{\mathcal{E}}$, including the error and phase recovery, can be written as $\tilde{E}_1 = \sqrt{\kappa\delta t} (\hat{\sigma}_k + iJ_k \delta t \sum_i \hat{\sigma}_{zk} \hat{\sigma}_{-i})$. Therefore, the final state after recovering the single-qubit errors is

$$\mathcal{R}[\tilde{\mathcal{E}}(\hat{\rho})] = \hat{\rho} + \mathcal{O}(\kappa\delta t)^2 + \mathcal{O}[(J\delta t)^2 \kappa\delta t]. \quad (\text{F6})$$

After the recovery process, the infidelity scales as $(\kappa t)^2$ for $J = 0$, and $(\kappa t)^2 + (Jt)^2 \kappa t$ otherwise. However, if κ is greater than J , then the $(\kappa t)^2$ part tends to dominate.

APPENDIX G: CHANNEL FIDELITY FOR A DISORDERED FIVE-QUBIT SETUP

To simulate physical setups, it is essential to take into account possible disorders in the qubit parameters. To this end, we consider a setup with variations in qubit frequencies and coupling strengths. Specifically, we introduce a 20% variation in each qubit frequency by keeping the average frequency of the qubits fixed, and likewise for each κ_j . Our results, shown in Fig. 6, demonstrate that the fidelity is relatively robust against such significant disorder.

- [1] F. Arute, K. Arya, R. Babbush, D. Bacon, J. C. Bardin *et al.*, Quantum supremacy using a programmable superconducting processor, *Nature (London)* **574**, 505 (2019).
- [2] H.-S. Zhong *et al.*, Quantum computational advantage using photons, *Science* **370**, 1460 (2020).
- [3] Y. Wu *et al.*, Strong quantum computational advantage using a superconducting quantum processor, *Phys. Rev. Lett.* **127**, 180501 (2021).
- [4] K. Bharti, A. Cervera-Lierta, T. H. Kyaw, T. Haug, S. Alperin-Lea, A. Anand, M. Degroote, H. Heimonen, J. S. Kottmann, T. Menke, W.-K. Mok, S. Sim, L.-C. Kwek, and A. Aspuru-Guzik, Noisy intermediate-scale quantum algorithms, *Rev. Mod. Phys.* **94**, 015004 (2022).
- [5] A. Montanaro, Quantum algorithms: An overview, *npj Quantum Inf.* **2**, 15023 (2016).
- [6] A. Peres, Reversible logic and quantum computers, *Phys. Rev. A* **32**, 3266 (1985).
- [7] P. W. Shor, Scheme for reducing decoherence in quantum computer memory, *Phys. Rev. A* **52**, R2493 (1995).
- [8] E. Knill and R. Laflamme, Theory of quantum error-correcting codes, *Phys. Rev. A* **55**, 900 (1997).
- [9] G. G. La Guardia, *Quantum Error Correction* (Springer, Cham, 2020).
- [10] E. Knill, R. Laflamme, and G. J. Milburn, A scheme for efficient quantum computation with linear optics, *Nature (London)* **409**, 46 (2001).
- [11] A. G. Fowler, A. M. Stephens, and P. Groszkowski, High-threshold universal quantum computation on the surface code, *Phys. Rev. A* **80**, 052312 (2009).
- [12] A. G. Fowler, Two-dimensional color-code quantum computation, *Phys. Rev. A* **83**, 042310 (2011).
- [13] A. G. Fowler, M. Mariantoni, J. M. Martinis, and A. N. Cleland, Surface codes: Towards practical large-scale quantum computation, *Phys. Rev. A* **86**, 032324 (2012).
- [14] R. Laflamme, C. Miquel, J. P. Paz, and W. H. Zurek, Perfect quantum error correcting code, *Phys. Rev. Lett.* **77**, 198 (1996).
- [15] D. G. Cory, M. D. Price, W. Maas, E. Knill, R. Laflamme, W. H. Zurek, T. F. Havel, and S. S. Somaroo, Experimental quantum error correction, *Phys. Rev. Lett.* **81**, 2152 (1998).
- [16] J. Chiaverini, D. Leibfried, T. Schaetz, M. D. Barrett, R. B. Blakestad, J. Britton, W. M. Itano, J. D. Jost, E. Knill, C. Langer, R. Ozeri, and D. J. Wineland, Realization of quantum error correction, *Nature (London)* **432**, 602 (2004).
- [17] P. Schindler, J. T. Barreiro, T. Monz, V. Nebendahl, D. Nigg, M. Chwalla, M. Hennrich, and R. Blatt, Experimental repetitive quantum error correction, *Science* **332**, 1059 (2011).
- [18] J. Cramer, N. Kalb, M. A. Rol, B. Hensen, M. S. Blok, M. Markham, D. J. Twitchen, R. Hanson, and T. H. Taminau, Repeated quantum error correction on a continuously encoded qubit by real-time feedback, *Nat. Commun.* **7**, 11526 (2016).
- [19] D. Ristè, S. Poletto, M.-Z. Huang, A. Bruno, V. Vesterinen, O.-P. Saira, and L. DiCarlo, Detecting bit-flip errors in a logical qubit using stabilizer measurements, *Nat. Commun.* **6**, 6983 (2015).
- [20] J. Kelly *et al.*, State preservation by repetitive error detection in a superconducting quantum circuit, *Nature (London)* **519**, 66 (2015).
- [21] Z. Chen *et al.*, Exponential suppression of bit or phase errors with cyclic error correction, *Nature (London)* **595**, 383 (2021).
- [22] M. H. Abobeih, Y. Wang, J. Randall, S. J. H. Loenen, C. E. Bradley, M. Markham, D. J. Twitchen, B. M. Terhal, and T. H. Taminau, Fault-tolerant operation of a logical qubit in a diamond quantum processor, *Nature (London)* **606**, 884 (2022).
- [23] L. Egan, D. M. Debroy, C. Noel, A. Risinger, D. Zhu, D. Biswas, M. Newman, M. Li, K. R. Brown, M. Cetina, and C. Monroe, Fault-tolerant control of an error-corrected qubit, *Nature (London)* **598**, 281 (2021).
- [24] C. K. Andersen, A. Remm, S. Lazar, S. Krinner, N. Lacroix, G. J. Norris, M. Gabureac, C. Eichler, and A. Wallraff, Repeated quantum error detection in a surface code, *Nat. Phys.* **16**, 875 (2020).
- [25] J. F. Marques, B. M. Varbanov, M. S. Moreira, H. Ali, N. Muthusubramanian, C. Zachariadis, F. Battistel, M. Beekman, N. Haider, W. Vlothuizen, A. Bruno, B. M. Terhal, and L. DiCarlo, Logical-qubit operations in an error-detecting surface code, *Nat. Phys.* **18**, 80 (2022).
- [26] C. Ryan-Anderson, J. G. Bohnet, K. Lee, D. Gresh, A. Hankin, J. P. Gaebler, D. Francois, A. Chernoguzov, D. Lucchetti, N. C. Brown *et al.*, Realization of real-time fault-tolerant quantum error correction, *Phys. Rev. X* **11**, 041058 (2021).
- [27] S. Krinner *et al.*, Realizing repeated quantum error correction in a distance-three surface code, *Nature (London)* **605**, 669 (2022).
- [28] Y. Zhao, Y. Ye, H. L. Huang, Y. Zhang, D. Wu, H. Guan, Q. Zhu, Z. Wei, T. He, S. Cao *et al.*, Realization of an error-correcting surface code with superconducting qubits, *Phys. Rev. Lett.* **129**, 030501 (2022).
- [29] N. Sundaresan *et al.*, Demonstrating multi-round subsystem quantum error correction using matching and maximum likelihood decoders, *Nat. Commun.* **14**, 2852 (2023).
- [30] R. Acharya *et al.*, Suppressing quantum errors by scaling a surface code logical qubit, *Nature (London)* **614**, 676 (2023).
- [31] C. Ryan-Anderson *et al.*, Implementing fault-tolerant entangling gates on the five-qubit code and the color code, [arXiv:2208.01863](https://arxiv.org/abs/2208.01863).
- [32] D. Gottesman, Stabilizer codes and quantum error correction, [arXiv:quant-ph/9705052](https://arxiv.org/abs/quant-ph/9705052).
- [33] I. L. Chuang, D. W. Leung, and Y. Yamamoto, Bosonic quantum codes for amplitude damping, *Phys. Rev. A* **56**, 1114 (1997).
- [34] M. H. Michael, M. Silveri, R. T. Brierley, V. V. Albert, J. Salmilehto, L. Jiang, and S. M. Girvin, New class of quantum error-correcting codes for a bosonic mode, *Phys. Rev. X* **6**, 031006 (2016).
- [35] H.-P. Breuer and F. Petruccione, *The Theory of Open Quantum Systems* (Oxford University Press, Oxford, 2007).
- [36] *Quantum Error Correction*, edited by D. A. Lidar and T. A. Brun (Cambridge University Press, Cambridge, 2014).
- [37] H.-P. Breuer, E.-M. Laine, J. Piilo, and B. Vacchini, Colloquium: Non-Markovian dynamics in open quantum systems, *Rev. Mod. Phys.* **88**, 021002 (2016).
- [38] V. Vadimov, J. Tuorila, T. Orell, J. Stockburger, T. Ala-Nissila, J. Ankerhold, and M. Möttönen, Validity of Born-Markov master equations for single- and two-qubit systems, *Phys. Rev. B* **103**, 214308 (2021).
- [39] W. S. Teixeira, F. L. Semião, J. Tuorila, and M. Möttönen, Assessment of weak-coupling approximations on a driven two-level system under dissipation, *New J. Phys.* **24**, 013005 (2022).
- [40] J. Tuorila, J. Stockburger, T. Ala-Nissila, J. Ankerhold, and M. Möttönen, System-environment correlations in qubit initialization and control, *Phys. Rev. Res.* **1**, 013004 (2019).

- [41] S. Alipour, A. T. Rezakhani, A. P. Babu, K. Mølmer, M. Möttönen, and T. Ala-Nissila, Correlation-picture approach to open-quantum-system dynamics, *Phys. Rev. X* **10**, 041024 (2020).
- [42] U. Weiss, *Quantum Dissipative Systems*, 3rd ed. (World Scientific, Singapore, 2008) Supplemental Material.
- [43] J. T. Stockburger and C. H. Mak, Stochastic Liouvillian algorithm to simulate dissipative quantum dynamics with arbitrary precision, *J. Chem. Phys.* **110**, 4983 (1999).
- [44] A. P. Babu, J. Tuorila, and T. Ala-Nissila, State leakage during fast decay and control of a superconducting transmon qubit, *npj Quantum Inf.* **7**, 30 (2021).
- [45] K. Georgopoulos, C. Emary, and P. Zuliani, Modeling and simulating the noisy behavior of near-term quantum computers, *Phys. Rev. A* **104**, 062432 (2021).
- [46] B. Schumacher, Sending entanglement through noisy quantum channels, *Phys. Rev. A* **54**, 2614 (1996).
- [47] V. V. Albert, K. Noh, K. Duivenvoorden, D. J. Young, R. T. Brierley, P. Reinhold, C. Vuillot, L. Li, C. Shen, S. M. Girvin, B. M. Terhal, and L. Jiang, Performance and structure of single-mode bosonic codes, *Phys. Rev. A* **97**, 032346 (2018).
- [48] D. Braun, F. Haake, and W. T. Strunz, Universality of decoherence, *Phys. Rev. Lett.* **86**, 2913 (2001).
- [49] A. F. Kockum, A. Miranowicz, S. D. Liberato, S. Savasta, and F. Nori, Ultrastrong coupling between light and matter, *Nat. Rev. Phys.* **1**, 19 (2019).
- [50] C. Lubich, *Integrators for Quantum Dynamics: A Numerical Analyst's Brief Review* (John von Neumann Institute for Computing, Jülich, 2002).